ping networks and technologies, J Lightwave Technol 18 (2000), 2058–2075.
3. N. Deng, Y. Yang, C.K. Chan, W. Hung, L.K. Chen, Intensity-modulated labeling and all-optical label swapping on angle-modulated optical packets, IEEE Photon Technol Lett 16 (2004), 1218–1220.
4. J. Yu and G.K. Chang, A novel technique for optical label and payload generation and multiplexing using optical carrier suppression and separation, IEEE Photon Technol Lett 16 (2004), 320–322.
5. J. Yu, G.K. Chang, and Q. Yang, Optical label generation, erasure, and reinsertion in a packet switched optical network using optical carrier suppression, separation, and wavelength conversion, IEEE Photon Technol Lett 16 (2004), 2156–2158.
6. T. Koonen, G. Morthier, et al., Optical packet routing in IP-over-WDM networks deploying two-level optical labeling, in Proc Eur Conf Optical Commun (ECOC2002), Copenhagen, Denmark, 2002, Paper 5.5.2.
7. N. Chi, B. Carlsson, P.V. Holm-Nielsen, C. Peucheret, and P. Jeppesen, Dispersion management for two-level optically labeled signals in IP-over-WDM networks, Presented at the ECOC'02, Copenhagen, Denmark, 2002, Paper 5.5.1.
8. C.W. Chow, H.K. Tsang, Optical label encoding and swapping using half-bit delayed dark RZ payload and DPSK label, Opt Exp 13 (2005), 5325–5330.
9. J. Yu, G.K. Chang, J. Barry, 40 Gbit/s signal format conversion from NRZ to RZ using a Mach-Zehnder delay interferometer, Opt Commun 248 (2005), 419–422.
10. C.-H. Cheng, The signal processing approach for the birefringent material based Mach-Zehnder interferometer design, Circuits Syst 1 (2005), pp. 211–214. 48th Midwest Symposium, Aug 7–10, 2005.
11. G.P. Agrawal, Fiber-optic communication systems, Wiley, New York, 1992, Chapter 4, pp. 133–178.

INTERNAL MEANDERED LOOP ANTENNA FOR GSM/DCS/PCS MULTIBAND OPERATION IN A MOBILE PHONE WITH THE USER'S HAND

Chun-I Lin and Kin-Lu Wong
Department of Electrical Engineering, National Sun Yat-Sen University, Kaohsiung 804, Taiwan, Republic of China

Received 22 August 2006

ABSTRACT: *A novel internal meandered loop antenna for application in a mobile phone for Global System for Mobile Communication/Digital Communication System/Personal Communication System (GSM/DCS/PCS) multiband operation is presented. Along the symmetric metal-strip loop structure of the antenna, there are meandered sections for adjusting the antenna's resonant frequencies and widened sections for improving the impedance matching. The antenna's first and second resonant modes (half- and one-wavelength modes) excited at about 900 and 1800 MHz for GSM/DCS operation. With the meandered sections in the loop structure, the antenna's third resonant mode (1.5-wavelength mode) can be adjusted to be close to the second resonant mode at 1800 MHz to achieve a wider upper band for DCS/PCS operation. In addition, the central region of the proposed loop antenna is unoccupied, which can be used to accommodate possible nearby electronic components, such as the lens of a digital camera. Furthermore, effects of the user's hand holding the mobile phone with the proposed loop antenna are analyzed in this study.* © 2007 Wiley Periodicals, Inc. Microwave Opt Technol Lett 49: 759–765, 2007; Published online in Wiley InterScience (www.interscience.wiley.com). DOI 10.1002/mop.22271

Key words: *mobile antennas; loop antennas; internal mobile phone antennas; GSM/DCS/PCS mobile phone antennas*

1. INTRODUCTION

Recently, owing to the rapid growth in mobile communications, the internal antennas for mobile devices are usually required to be capable of multiband operation. For this application, many related designs of the planar inverted-F antenna for application in mobile phones have been reported [1]. However, all the operating bands of the multiband PIFAs are with unbalanced structures and will thus lead to larger excited surface currents on the system ground plane than the antennas with self-balanced structures [2]. In this case, larger antenna performance degradation due to the user's adjacent effect than the antenna with self-balanced structures may be expected. For achieving the self-balanced structures, the modified one-wavelength loop antennas suitable to be placed on the system ground plane of the mobile phone have been presented [2–4]. These modified loop antennas, however, show mainly single-band operation and are with a two-layer or multilayer structure, which complicates the antenna configuration and increases the fabrication cost of the antenna.

In this paper, we present a novel internal meandered loop antenna (MLA) capable of operating in the Global System for Mobile Communication/Digital Communication System/Personal Communication System (GSM/DCS/PCS) bands for mobile phone applications. The proposed MLA is mainly with a one-layer symmetric metal-strip loop structure, which makes it easy to fabricate with a low cost. The antenna's lower operating band is formed by the antenna's first or fundamental resonant mode (half-wavelength mode), which covers the GSM (890–960 MHz) operation. For the upper operating band, it has a wide bandwidth covering the DCS (1710–1880 MHz) and PCS (1850–1990 MHz) operation, and is formed by the antenna's second resonant mode (one-wavelength mode) and third resonant mode (1.5-wavelength mode). A parametric study on adjusting the three resonant modes of the proposed MLA to achieve the desired lower and upper operating bands for GSM/DCS/PCS multiband operation is presented.

In addition, it is noted that among the antenna's three excited resonant modes, the second resonant mode is with a self-balanced structure, while the other two modes are with unbalanced structures. The antenna performances of the three resonant modes are discussed in this study. Further, the condition of the user's hand holding the mobile phone with the proposed MLA is considered, and effects of the user's hand on the antenna performances of the proposed MLA are analyzed.

2. ANTENNA DESIGN

Figure 1(a) shows the top view of the proposed MLA placed at the top portion of the system ground plane of a mobile phone. The system ground plane in this study is printed on a 0.8-mm thick FR4 substrate of size 45×100 mm^2, which is a reasonable size of general mobile phones. The MLA has a symmetric metal-strip loop pattern, which is cut from a 0.2-mm thick copper plate in the study. Note that, when there is no system ground plane, the MLA can only generate a one-wavelength resonant mode (the self-balanced mode). With the presence of the system ground plane, the MLA can generate additional half-wavelength and 1.5-wavelength resonant modes (the unbalanced modes). The successful excitation of the three resonant modes makes it possible to cover the GSM/DCS/PCS operation for the proposed antenna. This behavior will be analyzed in more detail with the aid of Figure 7 in section 3

Detailed dimensions of the metal-strip loop pattern in the planar structure are given in Figure 1(b). The dashed line shown in the figure is the bending line. The bending line separates the metal-strip loop pattern into two portions: the radiation portion and the feeding portion. The radiation portion is located above the

ground plane with a height (h) of 7 mm and mainly comprises two symmetric meandered sections and a widened central matching section of width (w) 4.5 mm and length 15 mm (matching section 1 in the figure). By adjusting the width w of matching section 1, enhanced impedance matching of the antenna's lower and upper bands can be obtained. Detailed effects of adjusting the width w will be discussed with the aid of Figure 4 in the next section. For the meandered sections, they can effectively lower the antenna's third resonant mode (1.5-wavlength mode) to be close to the second resonant mode (one-wavelength mode) to form a wide bandwidth at about 1800 MHz to cover the DCS/PCS operation. Effects of the meandered sections will be discussed in more detail with the aid of Figure 3. Also note that the achievable bandwidths of the antenna's lower and upper bands are greatly dependent on the height h of the MLA, and detailed results will be analyzed with the aid of Figure 6.

The feeding portion mainly has two symmetric widened matching sections of width 4 mm and length (t) 14 mm (matching section 2 in the figure), a 3-mm long feeding strip, and a 2.2-mm long shorting strip. Similar to the effects of the width w of matching section 1, by adjusting the length t of matching section 2, enhanced impedance matching of the antenna's lower and upper bands can be obtained. Detailed effects of tuning the length t on the antenna performances will be explored with the aid of Figure 5. For the feeding strip, it is connected at point A (the feeding point) to the 50-Ω microstrip line printed on the back side of the grounded FR4 substrate for testing the antenna in the experiment. For the shorting strip, it is directly short-circuited at point B (the shorting point) to the ground plane on the front side of the FR4 substrate.

Also note that, in the central region of the MLA, there is an unoccupied area of 15×13.5 mm^2. This unoccupied central region can be used to accommodate possible nearby electronic components, such as the lens or the CCD (charge coupled device) element of a digital camera [5, 6], leading to a compact integration of the MLA and nearby components. This possible application will be discussed in detail with the aid of Figure 8.

Furthermore, in this study, the proposed antenna and system ground plane are enclosed by a 1-mm thick plastic housing with relative permittivity (ε_r) 3.5 and conductivity (σ) 0.02 S/m [see Fig. 1(c)] to avoid their direct contact with the user's hand in the experiment. The thickness of the plastic housing is selected to be 17 mm, a reasonable thickness of general mobile phones. In addition, note that there is a 0.5-mm spacing between the antenna's radiation portion and the inner surface of the plastic housing. This small spacing can effectively decrease the loading effects of the plastic housing, making the radiation efficiency of the proposed antenna slightly affected. Effects of the user's hand holding the mobile phone with the proposed antenna are studied in Figures 9–12 and Tables 1–3.

TABLE 1 Simulated Results (Obtained From SEMCAD) of the Antenna Performances With the Presence of the User's Hand at 925 MHz

	$\eta_{radiation}$ (%)	$\eta_{mismatch}$ (%)	η (%)	Gain (dBi)	Directivity (dBi)
$d = 0$	25.9	75.3	19.5	−4.02	3.07
$d = 30$ mm	17.1	78.6	13.5	−4.53	4.16
$d = 60$ mm	49.2	99.7	49.1	−0.03	3.06
$d = 90$ mm	61.1	99.8	61.0	1.67	3.83
Free space	74.1	97.4	72.2	0.92	2.33

The radiation efficiency η is computed from $\eta_{radiation} \times \eta_{mismatch}$, where $\eta_{radiation}$ is the efficiency for the perfect matching condition and $\eta_{mismatch}$ is the efficiency decrease due to the frequency detuning caused by the presence of the user's hand.

TABLE 2 Simulated (SEMCAD) Results of the Antenna Performances With the Presence of the User's Hand at 1795 MHz

	$\eta_{radiation}$ (%)	$\eta_{mismatch}$ (%)	η (%)	Gain (dBi)	Directivity (dBi)
$d = 0$	27.3	98.9	27.0	−1.37	4.32
$d = 30$ mm	34.2	79.3	27.2	−1.68	3.97
$d = 60$ mm	53.7	96.7	51.9	0.67	3.52
$d = 90$ mm	58.7	96.7	56.8	1.06	3.52
Free space	70.3	94.5	66.5	1.95	3.72

3. RESULTS AND DISCUSSION

On the basis of the design dimensions shown in Figure 1, the proposed antenna was constructed and tested. Figure 2 shows the measured and simulated return loss of the constructed prototype enclosed by the plastic housing shown in Figure 1(c). The simulated results are obtained using Ansoft simulation software HFSS (high frequency structure simulator) (Ansoft Corporation HFSS, available at http://www.ansoft.com/products/hf/hfss/), and good agreement between the simulation and measurement is obtained. It is seen that three resonant modes at about 900, 1800, and 2000 MHz are successfully excited. From the measured results, the antenna's lower band formed by the first resonant mode or the half-wavelength mode has a bandwidth of 98 MHz (866–964 MHz), which covers the GSM operation. On the other hand, the antenna's upper band formed by the second and third resonant modes shows a large bandwidth of 480 MHz (1667–2147 MHz), which easily covers the DCS/PCS operation. Note that the bandwidth definition used in this study is 2.5:1 VSWR, which is a higher standard for practical mobile phone applications, because the internal antennas of general mobile phones are usually designed based on the bandwidth definition of 6 dB return loss (3:1 VSWR) or even less.

Next, to demonstrate the effects of the meandered sections in the proposed MLA, a comparison of the simulated return loss for the proposed antenna, folded loop antenna, and simple loop antenna is shown in Figure 3. Note that both of the lengths of the folded loop and simple loop antennas with a uniform strip width of 2.5 mm are selected to be about 178 mm, which is close to a half-wavelength of the frequency at 900 MHz. For the simple loop antenna, results indicate that three resonant modes with half-, one-, and 1.5-wavelength resonances are excited, although the impedance matching for frequencies over the first two modes needs to be improved. In addition, the simple loop antenna also occupies a large area in the system ground plane. By folding the simple loop structure, the folded loop antenna is obtained. In this case, smaller occupied area is achieved. Also, the antenna's first resonant mode

TABLE 3 Simulated (SEMCAD) Results of the Antenna Performances With the Presence of the User's Hand at 1920 MHz

	$\eta_{radiation}$ (%)	$\eta_{mismatch}$ (%)	η (%)	Gain (dBi)	Directivity (dBi)
$d = 0$	23.8	91.5	21.8	−2.23	4.39
$d = 30$ mm	36.5	97.6	35.7	−0.48	3.99
$d = 60$ mm	46.4	82.2	38.1	−1.18	3.01
$d = 90$ mm	46.6	82.8	38.6	0.12	4.26
Free space	69.9	80.9	56.6	2.63	5.10

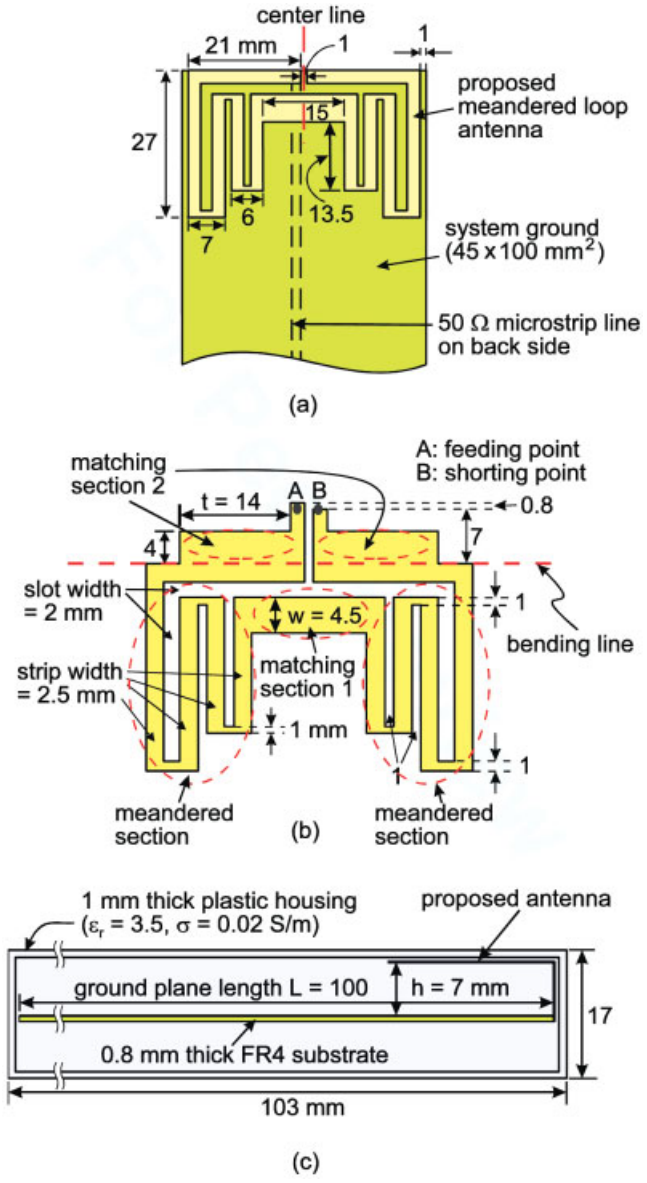

Figure 1 (a) Top view of the proposed internal MLA for GSM/DCS/PCS operation. (b) Detailed dimensions of the antenna in the planar structure. (c) Side view of the antenna enclosed by a 1-mm thick plastic housing. [Color figure can be viewed in the online issue, which is available at www.interscience.wiley.com]

is adjusted to be much closer to the desired frequency at about 900 MHz, and the third resonant mode is shifted to be closer to the second resonant mode. However, the second and third resonant modes are still too far away to form into a wide bandwidth. By further meandering the folded loop structure to achieve the proposed MLA shown in Figure 1, it is found that the antenna's third resonant mode can be adjusted to be very close to the second resonant mode to form a wide bandwidth to cover the DCS/PCS operation. Also, in this case, the antenna's first resonant mode is almost not affected.

Figures 4 and 5 show the effects of matching sections 1 and 2 on fine-tuning the resonant frequencies of the antenna's three excited resonant modes to achieve enhanced impedance matching of the antenna's lower and upper bands. In Figure 4, results for different widths (w varied from 2.5 to 5.5 mm) of matching section 1 are presented. It is seen that, with an increase in w, the second

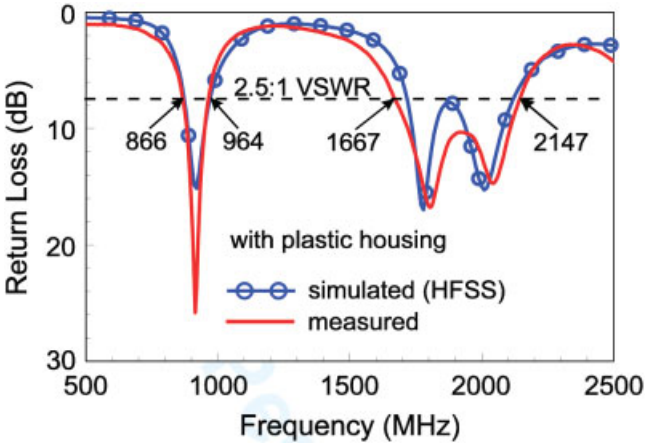

Figure 2 Measured and simulated (HFSS) return loss for the proposed antenna; the 1-mm thick plastic housing ($\varepsilon_r = 3.5$, $\sigma = 0.02$ S/m) is included in the study. [Color figure can be viewed in the online issue, which is available at www.interscience.wiley.com]

and third resonant modes are shifted to be closer to each other. For the case of width $w = 4.5$ mm, a wider bandwidth for the antenna's upper band is obtained. For this reason, the width w is thus selected to be 4.5 mm in the proposed antenna in this study. On the other hand, for the results of the length t varied from 0 to 19 mm shown in Figure 5, both the bandwidths of the antenna's lower and upper bands are in general increased with an increase in the length t. However, for the length $t = 19$ mm, the obtained bandwidth for the upper band is smaller than that of the length $t = 14$ mm. For this reason, the length t in the proposed antenna in this study is chosen to be 14 mm.

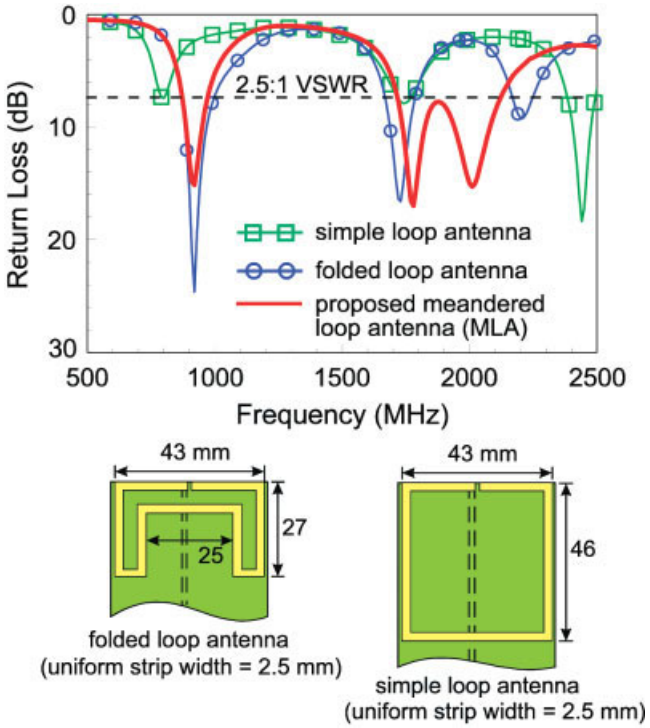

Figure 3 Simulated (HFSS) return loss for the proposed antenna, folded loop antenna, and simple loop antenna. [Color figure can be viewed in the online issue, which is available at www.interscience.wiley.com]

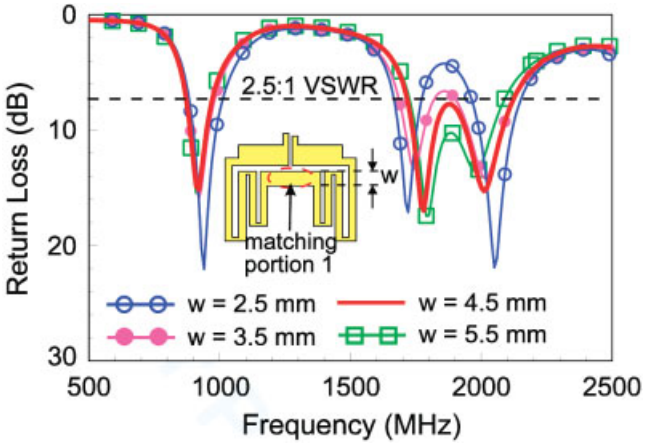

Figure 4 Simulated (HFSS) return loss as a function of w (width of matching section 1); other parameters are the same as in Figure 1. [Color figure can be viewed in the online issue, which is available at www.interscience.wiley.com]

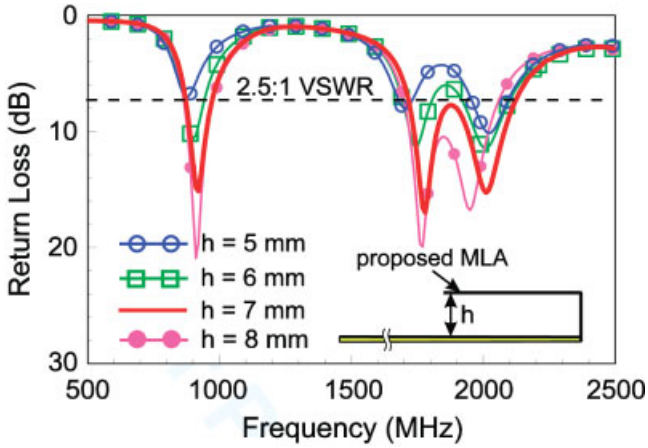

Figure 6 Simulated (HFSS) return loss as a function of h (height of the antenna); other parameters are the same as in Figure 1. [Color figure can be viewed in the online issue, which is available at www.interscience.wiley.com]

Effects of the antenna height h are also studied. Figure 6 shows the simulated return loss for the height h varied from 5 to 8 mm, with other dimensions of the antenna the same as given in Figure 1. From the results, it is seen that the resonant frequencies of the three resonant modes are generally about the same, only slightly affected by the height h. However, the achievable bandwidths for the antenna's lower and upper bands are generally larger with a larger value of the height h. With the consideration of achieving a lower height for the proposed antenna, h is selected to be 7 mm in this study.

Effects of the ground plane length L on the antenna performances are also studied. Figure 7 shows the simulated return loss for the cases with $L = 0$, 50, and 100 mm, and other dimensions of the antenna are the same as given in Figure 1. Results clearly indicate that the first and third resonant modes (unbalanced modes) will disappear when the ground plane length is decreased from 100 to 0 mm, only the second resonant mode (self-balanced mode) is successfully excited.

The possible integration of the lens or CCD element of the embedded digital camera in the central unoccupied region of the proposed antenna is also studied. To accommodate the lens of the digital camera, a hollow shielding metal cylinder of diameter 10 mm is placed in the central unoccupied region of the antenna. Note that the shielding metal cylinder has a height of 7 mm, the same as that of the antenna, and the distances of the shielding metal cylinder to the meandered sections and matching section 1 of the antenna are all 2.5 mm. The simulated results of the return loss are shown in Figure 8. From the results, it is seen that small variations in the impedance matching of the antenna are obtained, that is, effects of the shielding metal cylinder on the antenna performances are small and can be neglected. This behavior allows a compact integration of the proposed antenna and the nearby electronic components.

Finally, effects of the user's hand holding the mobile phone with the proposed antenna are studied. The experimental photo and simulation model are shown in Figure 9, in which the parameter d indicates the distance from the top edge of the mobile phone to the top of the user's thumb portion. From the measured and simulated return loss for $d = 0$, 30, 60, and 90 mm shown in Figures 9(a) and 9(b), agreement between the measurement and simulation is generally obtained. This agreement ensures reliable simulation results

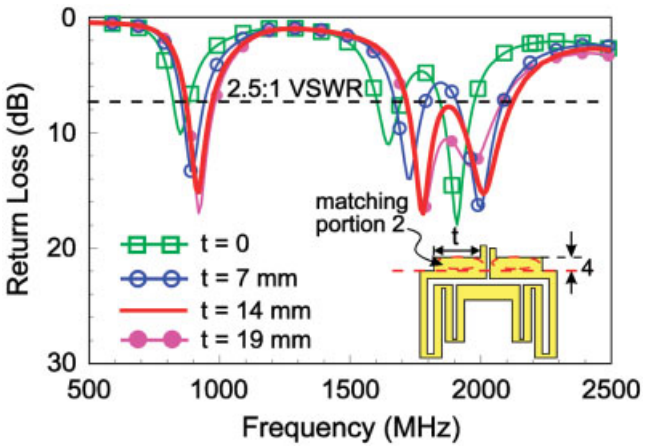

Figure 5 Simulated (HFSS) return loss as a function of t (length of matching section 2); other parameters are the same as in Figure 1. [Color figure can be viewed in the online issue, which is available at www.interscience.wiley.com]

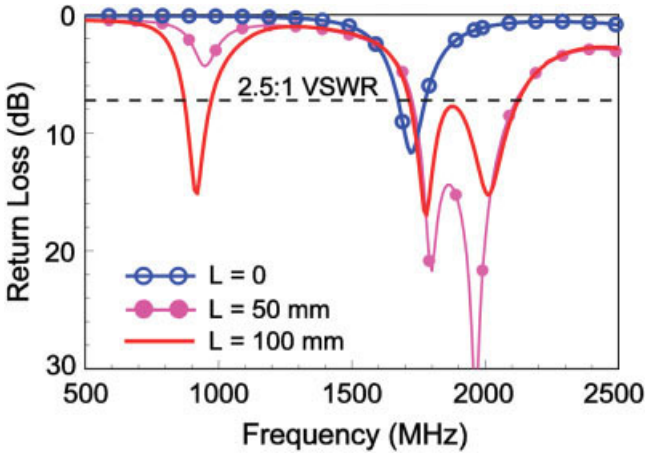

Figure 7 Simulated (HFSS) return loss as a function of L (length of the system ground plane); other parameters are the same as in Figure 1. [Color figure can be viewed in the online issue, which is available at www.interscience.wiley.com]

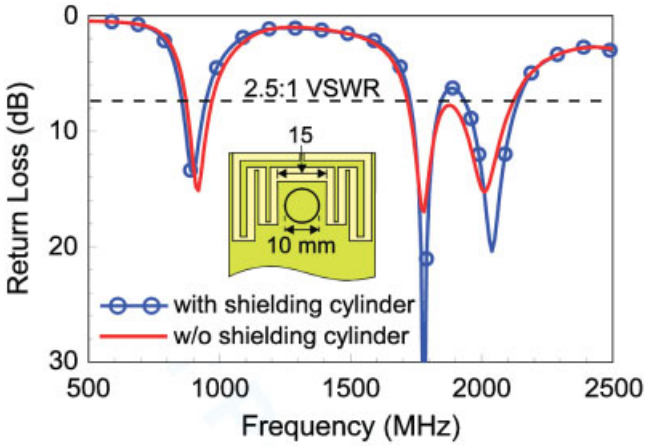

Figure 8 Simulated (HFSS) return loss for the case with the shielding metal cylinder. [Color figure can be viewed in the online issue, which is available at www.interscience.wiley.com]

obtained from the simulation hand model, which is provided by the commercial EM simulation software, SEMCAD (Schmid & Partner Engineering AG (SPEAG), available at http://www.semcad.com). The hand model mainly comprises the skin, muscle, and bones. The relative permittivity and conductivity of these tissues at 925, 1795, and 1920 MHz are obtained from Ref. 7. From the results shown in Figure 9, it is seen that there is frequency detuning for all the antenna's three resonant modes, when a certain portion of the antenna is overlaid by the user's hand ($d = 0$ and 30 mm). As for the case of $d = 60$ and 90 mm, in which the user's hand does not cover the proposed antenna, smaller frequency detuning for the three resonant modes is observed. The obtained results indicate that the performances of the proposed antenna are strongly dependent on the parameter d in this study.

Figures 10–12 show the simulated three-dimensional radiation patterns obtained from SEMCAD at 925, 1795, and 1920 MHz, the center frequencies of the GSM, DCS, and PCS bands. Note that, in order to obtain more accurate radiation patterns, the simulation hand model used here includes the user's forearm [8]. In Figures 10(a), 11(a), and 12(a), in which the distance $d = 0$, it is observed that the radiation power is greatly absorbed by the user's hand in the forearm direction, leading to a large distortion in the antenna's radiation patterns. Also, in each case, larger pattern distortion is seen when the distance d is smaller, that is, the user's hand is much closer to the proposed antenna in the mobile phone. With d increased to be 60 mm, the radiation patterns shown in Figures 10(c), 11(c), and 12(c) are restored to be similar to those in free space [Figs. 10(d), 11(d), and 12(d)]. It is also noted that the radiation patterns at 1795 MHz shown in Figure 11 for the second or self-balanced mode are also greatly distorted when the antenna is overlaid by the user's hand. The obtained results indicate that similar large pattern distortion will occur, which is mainly affected by the user's hand and is generally independent of the self-balanced or unbalanced modes excited by the proposed antenna.

The simulated radiation efficiency, antenna gain, and directivity as a function of d at 925, 1795, and 1920 MHz are also listed in Tables 1–3 for comparison. Owing to the presence of the user's hand, large decrease in the radiation efficiency is seen, and the radiation efficiency is generally decreased with a decrease in d. First note that, for the results at 925 MHz shown in Table 1, there is a large decrease in the radiation efficiency from 49.1% to less than 20% for d varied from 60 to 0 mm. This clearly suggests that, when the antenna is overlaid by a certain portion of the user's hand, large decrease in the radiation efficiency will occur. Similar large radiation efficiency decrease is seen for the results at 1795 and 1920 MHz shown in Tables 2 and 3, when d is varied from 60 to 0 mm.

It is also noted that at 1795 MHz, the radiation efficiency for $d = 60$ mm is only about 14.6% lower than that (51.9% vs. 66.5%) in free space (the user's hand not holding the mobile phone), which is smaller than the corresponding values at 925 and 1920 MHz (23.1% decrease from 72.2% in free space to 49.1% at $d = 60$ mm for 925 MHz, and 18.5% decrease from 56.6% in free space to

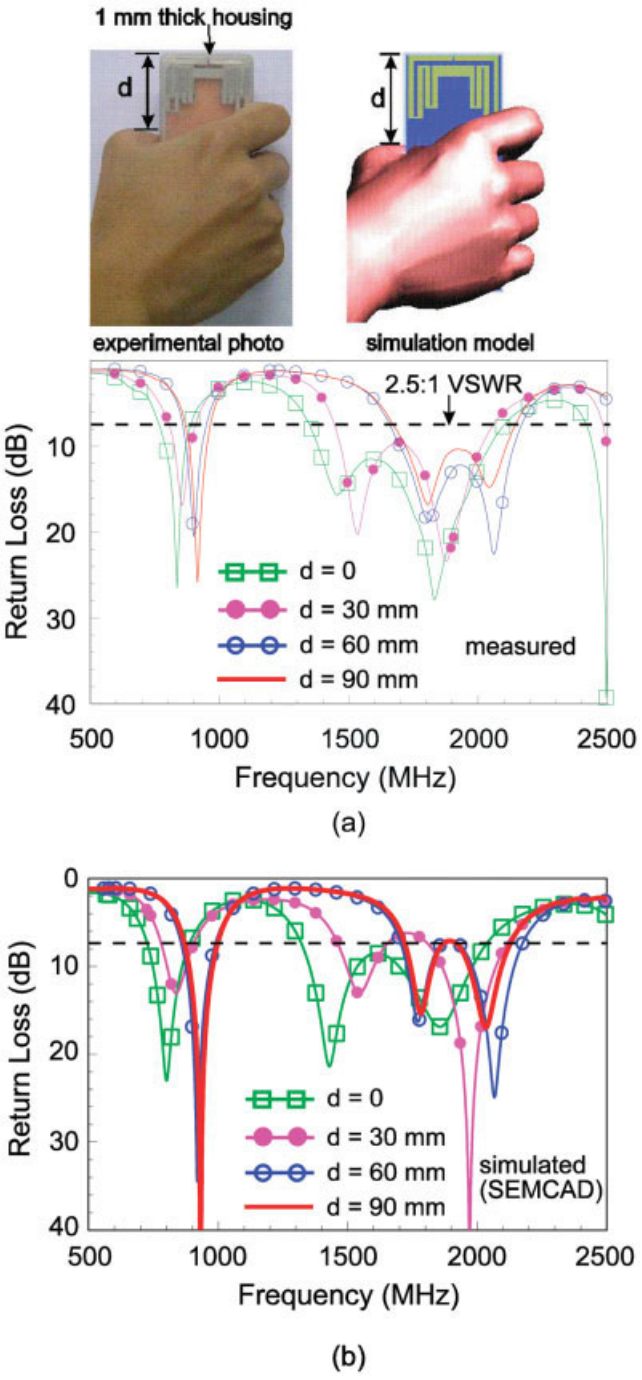

Figure 9 (a) Measured and (b) simulated (SEMCAD) return loss for $d = 0$, 30, 60, and 90 mm for the proposed antenna with the user's hand. [Color figure can be viewed in the online issue, which is available at www.interscience.wiley.com]

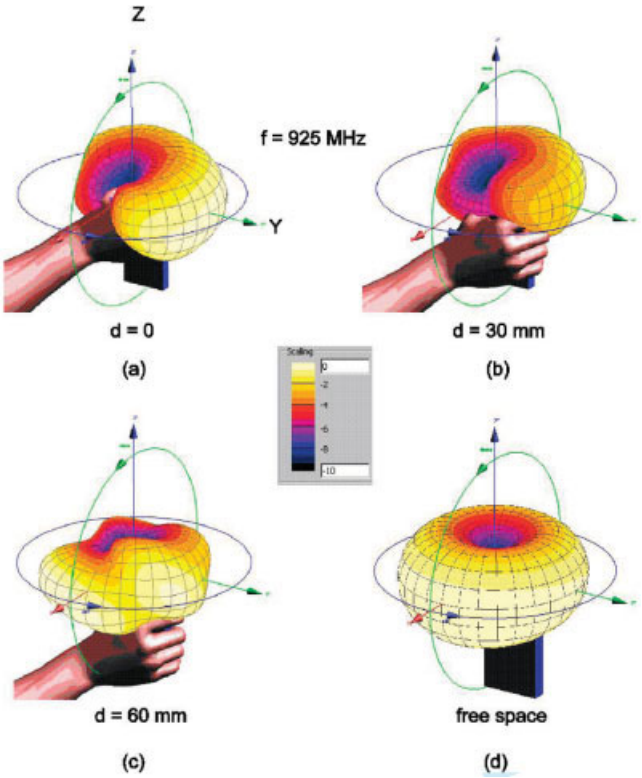

Figure 10 Simulated (SEMCAD) three-dimensional radiation patterns at 925 MHz. [Color figure can be viewed in the online issue, which is available at www.interscience.wiley.com]

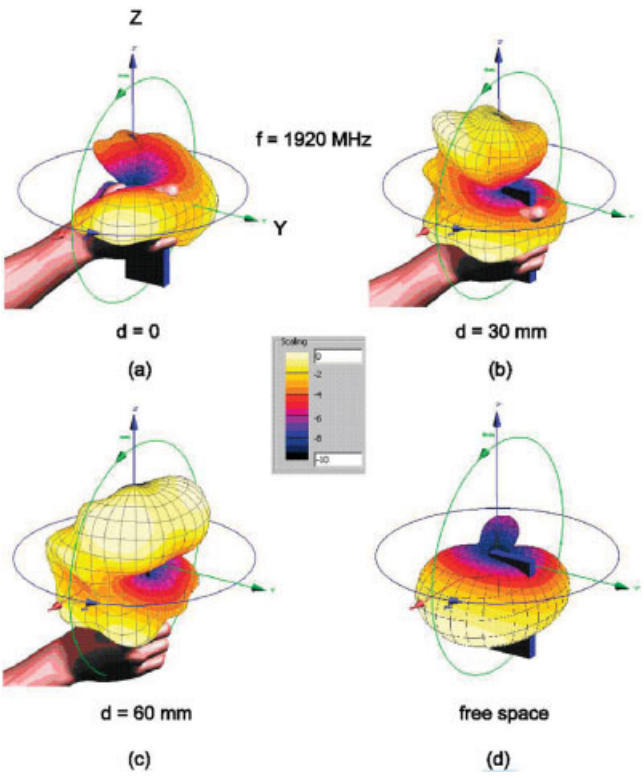

Figure 12 Simulated (SEMCAD) three-dimensional radiation patterns at 1920 MHz. [Color figure can be viewed in the online issue, which is available at www.interscience.wiley.com]

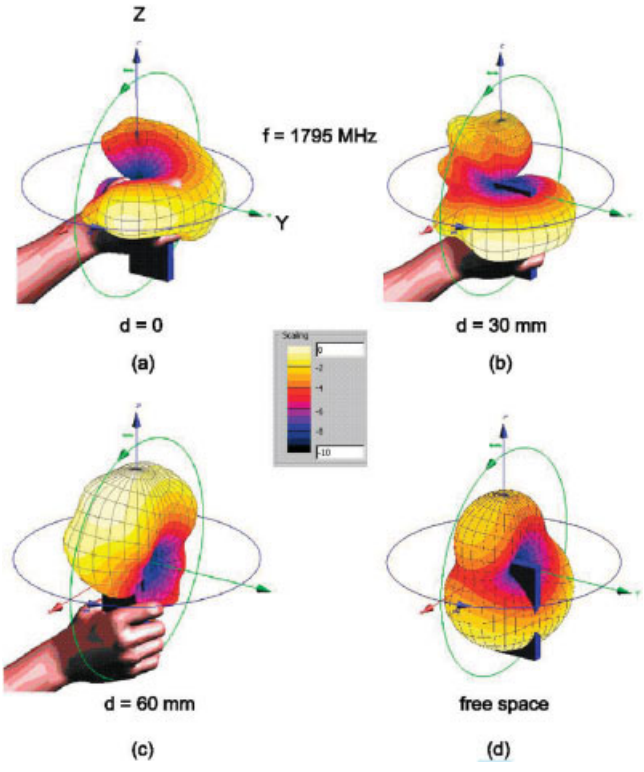

Figure 11 Simulated (SEMCAD) three-dimensional radiation patterns at 1795 MHz. [Color figure can be viewed in the online issue, which is available at www.interscience.wiley.com]

38.1% at $d = 60$ mm for 1920 MHz). In this case, the smaller efficiency decrease at 1795 MHz is probably owing to the smaller excited surface currents in the system ground plane for the proposed antenna operated in the self-balanced resonant mode [2].

4. CONCLUSIONS

A novel internal MLA capable of GSM/DCS/PCS multiband operation in the mobile phone has been proposed and studied. The proposed antenna is mainly with a one-layer metal-strip loop structure, which makes it easy to fabricate with a low cost. For the proposed antenna, three resonant modes including two unbalanced modes (half- and 1.5-wavlength modes) and one self-balanced mode (one-wavelength mode) have been successfully excited. The three resonant modes are formed into two wide bands covering GSM and DCS/PCS operation. The fine-tuning of the resonant frequencies and improvement in the impedance matching of the antenna's three resonant modes have been studied. Effects of the user's hand holding the mobile phone with the proposed antenna have also been analyzed. Strong effects of the user's hand on the impedance and radiation characteristics of the antenna have been observed. Results also indicate that, when the user's hand is close to or cover a certain portion of the antenna, large decrease in the antenna's radiation efficiency and great distortion in the antenna's radiation pattern will occur. In this condition (d smaller than 60 mm in this study), strong user's hand effects have been observed for all the three excited resonant modes of the antenna. On the other hand, when the user's hand holds the mobile phone with a large distance to the proposed antenna ($d = 60$ mm or larger), smaller decrease in the radiation efficiency has been observed for the antenna's second resonant mode (one-wavelength self-balanced mode) than the antenna's two other unbalanced modes (half- and 1.5-wavelength modes). This behavior is largely because, in

this condition, the excited surface currents in the system ground plane is smaller for the proposed antenna operated in the self-balanced resonant mode.

REFERENCES

1. K.L. Wong, Planar antennas for wireless communications, Wiley, New York, 2003, Chapter 2.
2. H. Morishita, Y. Kim, and K. Fujimoto, Design concept of antennas for small mobile terminals and the future perspective, IEEE Antennas Propag Magn 44 (2002), 30–43.
3. H. Morishita, H. Furuuchi, and K. Fujimoto, Performance of balanced-Fed antenna system for handsets in the vicinity of a human head or hand, IEE Proc Microwave Antennas Propag 149 (2002), 85–91.
4. S. Hayashida, T. Tanaka, H. Morishita, Y. Koyanagi, and K. Fujimoto, Built-in folded monopole antenna for handsets, Electron Lett 39 (2004), 1514–1516.
5. S.L. Chien, F.R. Hsiao, Y.C. Lin, and K.L. Wong, Planar inverted-F antenna with a hollow shorting cylinder for mobile phone with an embedded camera, Microwave Opt Technol Lett 41 (2004), 418–419.
6. K.L. Wong, S.L. Chien, C.M. Su, and F.S. Chang, An internal planar mobile phone antenna with a vertical ground plane, Microwave Opt Technol Lett 47 (2005), 597–599.
7. S. Gabriel, R.W. Lau, and C. Gabriel, The dielectric properties of biological tissues. III. Parametric models for the dielectric spectrum of tissues, Phys Med Biol 41 (1996), 2271–2293.
8. C.M. Su, C.H. Wu, K.L. Wong, S.H. Yeh, and C.L. Tang, User's hand effects on EMC internal GSM/DCS dual-band mobile phone antenna, Microwave Opt Technol Lett 48 (2006),1563–1569.

TUNABLE AND INJECTION-SWITCHABLE ERBIUM-DOPED FIBER LASER OF LINE STRUCTURE

Daru Chen,[1,2] Shan Qin,[1,2] Zhangwei Yu,[1,2] and Sailing He[1,2,3]
[1] Centre for Optical and Electromagnetic Research, Zhejiang University, Hangzhou 310058, China
[2] Joint Research Center of Photonics of the Royal Institute of Technology (Sweden) and Zhejiang University, East Building No. 5, Zhejiang University, Hangzhou 310058, China
[3] School of Electrical Engineering, Royal Institute of Technology

Received 28 August 2006

ABSTRACT: *A tunable and injection-switchable erbium-doped fiber (EDF) laser is proposed based on a line structure formed by a fiber Sagnac loop reflector and an fiber Bragg grating (FBG). Wavelength switching is achieved by controlling the power of the tunable injection laser. The self-seeded wavelength corresponding to the Bragg wavelength of the FBG can be tuned by, for example, heating the FBG, and the injection wavelength can be tuned over a wide range of about 50 nm. The characteristics of the wavelength switching for different levels of the EDF pump power and different wavelengths of the injection laser are studied experimentally. The present fiber laser has the advantages of tunability, stability, low amplified spontaneous emission noise, and high injection efficiency when compared with a fiber ring laser. Rapid wavelength switching is expected and the transient switching response of the laser is also studied.* © 2007 Wiley Periodicals, Inc. Microwave Opt Technol Lett 49: 765–768, 2007; Published online in Wiley InterScience (www.interscience.wiley.com). DOI 10.1002/mop.22262

Key words: *tunable; injection; switchable; line structure; Erbium-doped fiber laser*

1. INTRODUCTION

Wavelength-switchable and tunable fiber lasers have important applications in WDM fiber communication systems, fiber sensors, and so forth. Several techniques have been reported to achieve wavelength switching in fiber lasers, such as the use of sampled fiber Bragg gratings (FBG) [1], cascaded FBGs [2, 3], a Sagnac loop reflector [4], a few-mode fiber grating [5], a slanted multimode FBG [6], a Bragg grating-based acoustooptic superlattice modulator [7], a hybrid gain medium [8], a multi-section high-birefringence fiber loop mirror [9], a programmable electric-actuated polarization controller [10], and hybrid pumps [11]. Overlapping cavities can be used for multi-wavelength lasing and wavelength switching can be achieved by controlling the loss or the gain in different cavities [2, 3, 11]. Recently, Dragic and coworkers have reported an injection-seeded erbium-doped fiber (EDF) ring laser [12–14], in which an injection technique was used to achieve a wavelength-switchable fiber laser. A tunable laser (outside the cavity of the fiber laser) is used as seeding light. The shared cavity is for self-seeded lasing or injection-seeded lasing. Switching between the self-seeded wavelength lasing and injection-seeded wavelength lasing can be achieved by controlling the power of the injection laser. By using this technique, one of the switching wavelengths can be tuned among a large range since a tunable injection laser is employed.

In this article we propose a novel tunable and switchable EDF laser of line structure [see Fig. 1(a)]. Here a fiber Sagnac loop reflector and an FBG are employed to form a line cavity (like a Fabry-Perot cavity). The seeding light is injected into the cavity through an optical circulator. Dual-wavelength switching is achieved by controlling the power of the injection laser. One wavelength corresponds to the Bragg wavelength of the FBG (can be tuned by changing the temperature or stress) and the other wavelength can be tuned from 1535 to 1590 nm (determined by the wavelength of the injection laser).

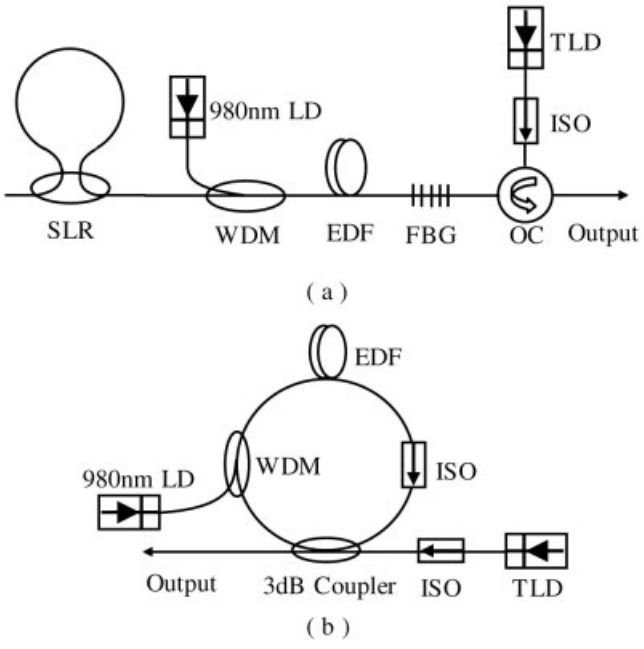

Figure 1 The schematic configuration of (a) the proposed tunable and injection-switchable fiber laser of line structure and (b) a fiber ring laser similar to the one proposed in Ref. 13. LD, laser diode; TLD, tunable laser diode; WDM, wavelength division multiplexing; FBG, fiber Bragg grating; OC, optical circulator; ISO, isolator; EDF, erbium-doped fiber; SLR, Sagnac loop reflector